

Journal of Materials Chemistry A

Accepted Manuscript



This is an *Accepted Manuscript*, which has been through the Royal Society of Chemistry peer review process and has been accepted for publication.

Accepted Manuscripts are published online shortly after acceptance, before technical editing, formatting and proof reading. Using this free service, authors can make their results available to the community, in citable form, before we publish the edited article. We will replace this *Accepted Manuscript* with the edited and formatted *Advance Article* as soon as it is available.

You can find more information about *Accepted Manuscripts* in the [Information for Authors](#).

Please note that technical editing may introduce minor changes to the text and/or graphics, which may alter content. The journal's standard [Terms & Conditions](#) and the [Ethical guidelines](#) still apply. In no event shall the Royal Society of Chemistry be held responsible for any errors or omissions in this *Accepted Manuscript* or any consequences arising from the use of any information it contains.

COMMUNICATION

Radar like Iron based Nanohybrid as Efficient and Stable Electrocatalyst for Oxygen Reduction

Cite this: DOI: 10.1039/x0xx00000x

Xing Zhong,^a Lin Liu,^a Xinde Wang,^a Huiyou Yu,^a Guilin Zhuang,^a Donghai Mei,^b Xiaonian Li,^a Jian-guo Wang^{*a}Received 00th January 2012,
Accepted 00th January 2012

DOI: 10.1039/x0xx00000x

www.rsc.org/

A new type of hybrid material consisting of iron phthalocyanine (FePc) coordinated with pyridyne cycloaddition of graphene sheets (PyNG) as a high-performance electrocatalyst for ORR were fabricated. The Fe-PyNG hybrid has a similar overpotential but has a higher current density and superior stability than Pt/C in alkaline solutions for ORR.

Proton exchange membrane fuel cells (PEMFCs) are promising candidates for clean and efficient energy conversion amidst the impending global energy crisis.¹⁻³ Catalysts for oxygen reduction reactions (ORR) are the major focus of chief renewable energy technologies in fuel cells. It has been well known that Pt and its alloy are known as efficient catalysts for ORR; however, the prohibitive cost and scarce reserves of Pt have hampered the widespread use of PEMFCs.^{4,5} For the sustainable commercialization of PEM fuel cells, researchers have conducted intense research into the development of efficient and inexpensive alternatives to Pt-based catalysts.⁶⁻¹² Since Jasinski and Yeager's pioneering works,^{13,14} an increasing number of research have focused on non-precious metal ORR catalysts based on pyrolyzed and non-pyrolyzed transition metal macrocycles (M-Nx-C). In this regard, the unprecedented catalytic activity and power density of pyrolyzed Fe- and Co-based electrocatalysts have made them promising alternative to Pt-based catalysts.¹⁵⁻¹⁸ Nonetheless, the activity and durability of pyrolyzed M-Nx-C catalysts strongly depend on complex preparation methods, which make it very difficult in tailoring the structure and surface properties extremely difficult. Meanwhile, few non-pyrolyzed M-Nx-C catalysts have reached the level of Pt-based catalysts. The big challenges of non-pyrolyzed M-Nx-C catalysts are the stability. Although great progress has been achieved in this area, their catalytic performance remains unsatisfactory; in addition, the exact reaction mechanism of these non-precious metal catalysts remains controversial despite tremendous efforts.¹⁹⁻²² Thus, novel and sophisticated strategies for material synthesis are highly desirable for achieving cost-effective ORR electrocatalysts with high activity and stability. In addition,

identifying the nature of real active sites and elucidating the catalysis mechanism are also required.

The use of hybrid materials is a new approach of fabricating high-performance electrocatalysts; however, very limited success is noted in developing a controllable assembly of non-precious metal growth or coordination on an active support as synergistic ORR catalysts.²³⁻²⁵ Moreover, the synergetic effects of their active sites in the hybrids are not fully determined. Recent studies have implied that iron phthalocyanine (FePc) provides the best activity among transition metal N4-macrocycles. Unfortunately, the drawback of FePc molecules is easy aggregation; thus, the catalytic activity and stability still remain unsatisfactory to match that of Pt.²⁶⁻²⁸ Recently, Cho reported FePc coordination with a vertical single-bond pyridine anchored on carbon nanotubes, thereby demonstrating the good electrocatalytic activity for ORR.²⁹ Loh reported a hybrid by reacting the pyridine-functionalized graphene with iron-porphyrin, a graphene-metalloporphyrin MOF with enhanced catalytic activity for ORR.³⁰ Our recent study has demonstrated that the pyridyne cycloaddition of graphene sheets (PyNG) can provide an "external" active site for ORR with good stability due to the strong interaction between pyridine and graphene.³¹ Because the coordination bond between pyridine-N and FePc is strong,^{32,33} thus, we propose that pyridine-N in PyNG can be an available anchor to enable intimate coupling and interactions with the FePc iron center, which will form effective and strongly coupled Fe-N-C hybrids.

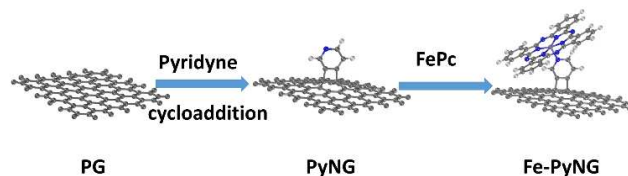


Fig. 1 Schematic illustration of the fabrication of Fe-PyNG hybrids.

Based on this design concept, we report a novel hybrid material composed of FePc anchored on PyNG as a high-performance catalyst for ORR. Although FePc or PyNG alone has moderate catalytic activity, their hybrid exhibits an unexpected high ORR activity. The Fe-PyNG hybrid has a similar overpotential but has a higher current density and superior stability than Pt/C in alkaline solutions for ORR. Physical mixtures of FePc with pristine graphene (PG) also have lower ORR activities than corresponding hybrid materials. This finding suggests that synergistic coupling effects between FePc and PyNG are indispensable to a high ORR activity. Fortunately, the precise control of interactions between FePc and PyNG facilitates an in-depth understanding of the reaction mechanism. On the basis of density functional theory (DFT) calculations, it is found that N-modified Fe is a highly active site for the adsorption of OOH and ORR reaction due to the pronounced charge transfer from Fe to N. Meanwhile, the strong chemical bonding between FePc and pyridine in PyNG leads to its high stability. The existence of Fe-N-C mainly results in the high electrochemical activity of the Fe-PyNG hybrid.

The fabrication process for Fe-PyNG hybrid is demonstrated in Fig. 1. PyNG was prepared through a one-step mild chemical modification process, as previously reported.³¹ Taking advantage of the pyridyne cycloaddition, pyridine becomes an exposed anchor. Fe-PyNG was prepared by refluxing the PyNG and FePc mixture in N, N-dimethylformamide (DMF) in an Ar atmosphere. Both PyNG and FePc exhibited significantly good dispersibility in DMF, thus, FePc can be easily coordinated to PyNG through the bond formed between the N atom in pyridine and the Fe center in FePc. As a reference point, the FePc/pristine graphene hybrid (Fe-PG) was also prepared by following the same procedure for comparison, but PG is used instead of PyNG. The first question is if FePc was covalently anchored on PyNG. Confirming how the combined action of FePc and PyNG influences the chemical structure and electrocatalytic performance of the hybrid is important.

The nanosheet morphologies of PG, Fe-PyNG, and Fe-PG were investigated via transmission electron microscopy (TEM) and atomic force microscopy (AFM). Continuous silk wave morphology associated with PG was easily observed (Fig. S1a and S1b). The AFM results show that the measured thickness of the PG layer is around 0.8 nm to 1.0 nm (Fig. S1c and S1d), which can be ascribed to few-layer graphene sheets. The TEM image (Fig. 2a) of Fe-PyNG shows the uniform dispersion of FePc nanoparticles over the PyNG surface. For comparison, the TEM images of FePc that was directly loaded on PG are shown in Fig. 2b. Some dot-like nanoparticles were observed in the TEM images of Fe-PyNG and Fe-PG. However, the population of FePc adsorbed on PG-based π - π interaction is more than those that were covalently attached on PyNG. Such phenomenon implies that the effect of the strong coupling between FePc and PyNG can decrease agglomeration, which results in better dispersion and considerably reduced particle sizes of FePc.

To investigate the PG, PyNG, Fe-PyNG, and Fe-PG hybrids further, Raman spectra are included in Fig. 2c for comparison in terms of the ratio of D (1333 cm^{-1}) and G (1600 cm^{-1}) band intensities. The ratio between D and G band intensities (I_D/I_G) was used as an indication of the level of defects that are present within

the samples. After pyridyne cycloaddition, the D band shifted to 1327 cm^{-1}

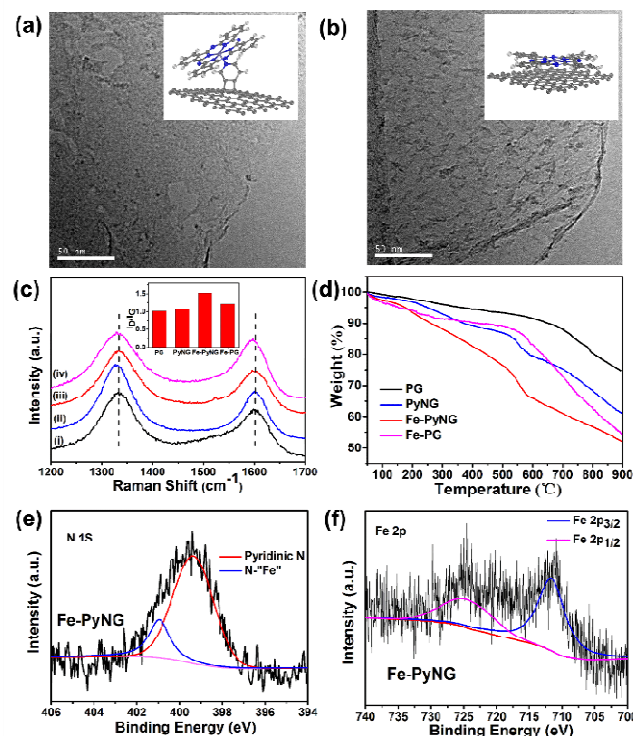


Fig. 2 (a) HRTEM image of Fe-PyNG; (b) HRTEM image of Fe-PG; (c) Raman spectra of (i) PG, (ii) PyNG, (iii) Fe-PyNG, and (iv) Fe-PG hybrid; (d) TGA thermograms of PG, PyNG, Fe-PyNG, and Fe-PG hybrid; (e) N 1s, and (f) Fe 2p XPS survey spectra of Fe-PyNG.

compared with the PG (1333 cm^{-1}). The I_D/I_G ratio of the PyNG (1.08) is slightly higher than that of the initial PG (1.02). In addition, compared with PG and PyNG, the Fe-PyNG spectra revealed a more intense D band (I_D/I_G approximately 1.52). This relative shift sufficiently suggests a strong interaction between FePc and PyNG, which can be attributed to the synergistic effect of FePc and PyNG. Moreover, the I_D/I_G ratio of Fe-PG is 1.21, which slightly varies with PG. This finding indicates that the π - π interactions between FePc and PG did not distort the sp^2 carbon lattice of the graphene.

Fig. 2d shows the thermogravimetric analysis (TGA) curves of the PG, PyNG, Fe-PyNG, and Fe-PG hybrids obtained at a heating rate of $10\text{ }^\circ\text{C}/\text{min}$ in Ar. PG shows a weight loss (25%), which can be attributed to the removal of oxygen-containing functional groups (such as $-\text{OH}$) as well as the disintegration of the graphene structure from PG. The weight loss of Fe-PG is calculated to be 45%, and the mass loss observed at $500\text{ }^\circ\text{C}$ is attributed to the FePc assembled on PG. The weight loss of PyNG is calculated to be about 39% when subjected to two continuous decompositions at $500\text{ }^\circ\text{C}$. This finding is presumably due to pyridine group decomposition. Fe-PyNG has a similar decline curve with PyNG but has more weight loss (48%). This loss may have originated from the breakdown of the coordination bond between FePc and PyNG. Based on this observation, we estimated that the molar ratio of pyridine to graphene carbon is calculated to be 1:40 in PyNG, and the average ratio of FePc coupling to pyridine-N in the Fe-PyNG hybrid is 1:10.

Based XPS analysis, the element contents of these materials were determined and are summarized in Table S1. Atom % N of

0.35 was noted in PG, and such a slight content of N did not influence the electrocatalysis results in this work. As expected, 3.58 atom % pyridine-N was found in PyNG, which is similar with the results of our previous report.³¹ The XPS results of Fe-PyNG and Fe-PG suggested the presence of Fe, C, N, and O components in the hybrids (Fig. S2 and S3). The high-resolution N1s spectrum of the Fe-PyNG sample provided further evidence for the incorporation of Fe ion and pyridinic-N (Fig. 2e). Notably, we found two peaks located at approximately 400.9 and 399.4 eV for Fe-PyNG, which can be attributed to N-Fe bonding and pyridine-N structures.³⁴⁻³⁷ However, the N1s spectrum of Fe-PG (Fig. S4d) is almost the same as that of FePc (Fig. S5). Emphasizing that no additional peak was observed is important. The new peak at 400.9 eV of Fe-PyNG indicates that new chemical bonds were formed, which provides efficient coordination between Fe and pyridinic-N. This finding indicates that Fe-N-C active sites were established at Fe-PyNG. Furthermore, 0.31 atom % Fe was estimated to be present in the Fe-PyNG hybrid as well as two peaks at 724.5 and 710.8 eV, which may be assigned to Fe 2p_{1/2} and Fe 2p_{3/2} for Fe-PyNG, respectively (Fig. 2f and S6). Based on the values of Fe content in Fe-PyNG, we calculated that the ratio of FePc coordinated to PyNG was approximately 1:11, which is consistent with the estimation from the TGA results. In addition, the Fe content in Fe-PG was determined to be 0.34 atom %, which is close with that in Fe-PyNG. This result implies that the FePc content is nearly at the same level in Fe-PyNG and Fe-PG, which may provide a more equitable environment for electrocatalytic performance evaluation.

To demonstrate the advantages of the Fe-PyNG hybrid in ORR, we first examined the electrocatalytic properties of PG, PyNG, Fe-PyNG, and Fe-PG in a N₂- and O₂-saturated 0.1 M aqueous KOH electrolyte solution at a constant active mass loading and a scan rate of 100 mV s⁻¹ (Fig. 3a). As a basis for comparison, the ORR activity of Fe-PyNG was compared with that of commercial 20 % Pt/C catalyst at the same conditions. Apparently, Fe-PyNG exhibited a significantly higher ORR mass activity associated with a more positive ORR onset potential (-0.03 V) and higher current density (-3.54 mA cm⁻²) than Fe-PG (-0.07 V, -2.69 mA cm⁻²) and PyNG (-0.16 V, -3.18 mA cm⁻²) (Fig. S7). Moreover, the current density of Fe-PyNG is higher than that of the Pt/C catalyst (Fig. S8). Notably, a small acromion at -0.35 V to -0.45 V was observed in Fe-PG, which can be attributed to the original PG catalytic behavior (Fig. S9). On the contrary, this acromion did not appear in Fe-PyNG. This finding suggests that the incorporation of pyridine-N and Fe ion of FePc provided a unique chemical and electronic structure. In addition, this incorporation is primarily responsible for the positive shift of the onset potential as well as the high current density of Fe-PyNG.

Subsequently, to examine the reaction kinetics for PG, PyNG, Fe-PyNG, and Fe-PG electrodes, linear sweep voltammograms (LSVs) were recorded in an O₂-saturated 0.1 M KOH electrolyte at a scan rate of 10 mV s⁻¹ by using a rotating disk electrode (RDE) (Fig. 3b, S10, and S11). As displayed in Fig. 3b, the Fe-PyNG catalyst exhibits an unexpectedly high ORR activity (with an onset potential as low as -0.03 V) that was comparable to that of commercial Pt/C (-0.01 V) during oxygen reduction (Fig. S12). Furthermore, the half-wave potential (E_{1/2}) of the Fe-PyNG catalyst is more positive by about 30 mV than that of commercial Pt/C; in addition, its limited diffusion current is comparable to that of Pt/C (Fig. S13). By contrast, the E_{1/2} values of Fe-PG and PyNG are much lower than

that of Fe-PyNG. The results are in agreement with the CV observations, which indicates that Fe-PyNG has a superior electrocatalytic activity toward ORR. The favourable ORR activity of Fe-PyNG is also revealed from

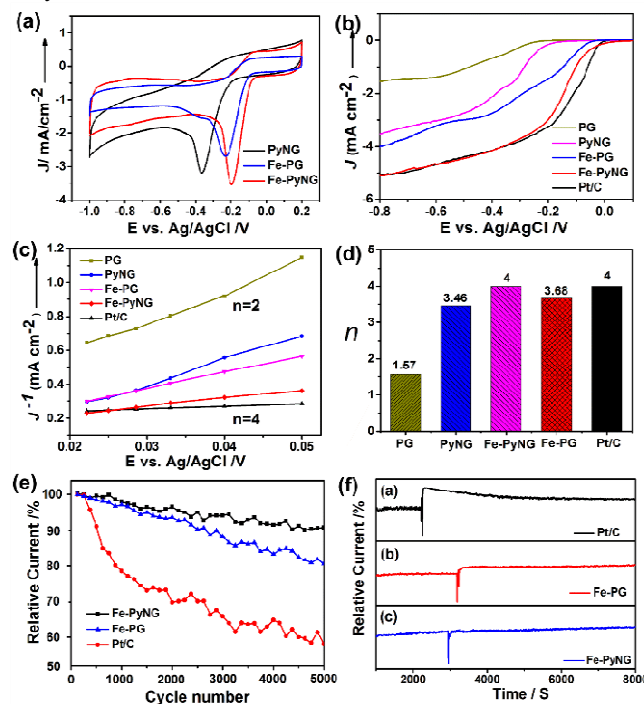


Fig. 3 (a) CVs (100 mV s⁻¹) of PyNG, Fe-PyNG, and Fe-PG in O₂-saturated 0.1 M KOH; (b) LSV curves (10 mV s⁻¹) on an RDE (1600 rpm) in an O₂-saturated 0.1 M KOH solution; (c) Koutecky–Levich plots of PG, PyNG, Fe-PyNG, and Fe-PG at -0.6 V; (d) Endurance test of Fe-PyNG, Fe-PG, and Pt/C for 5000 cycles in 0.1 M KOH; (e) Electron transfer numbers of PG, PyNG, Fe-PyNG, and Fe-PG at -0.6 V; (f) Methanol crossover tolerance test by chronoamperometric response in 0.1 M KOH aqueous electrolyte.

the Tafel plots (Fig. S14). The number of electrons transferred through the Fe-PyNG catalyzed electrocatalytic reaction was then determined using the Koutecky–Levich plots and is displayed in Fig. 3c. The corresponding Koutecky–Levich plots at an electrode potential of -0.6 V revealed that Fe-PyNG exhibited a high ORR current that is extremely close to that of the commercial Pt/C catalyst and is significantly higher than those of Fe-PG and PyNG. We conclude that the incorporation of pyridine-N and Fe ion should be the key factor in the enhancement and domination of ORR activity increase. The transferred electron number *n* of Fe-PyNG, Fe-PG, and PyNG exceeds 3 (Fig. 3d). This finding shows that the oxygen reduction in all three catalysts followed the four-electron transfer pathway.

The long term stabilities of the catalysts were determined by CV cycling in an O₂ saturated 0.1 M KOH solution between -1 and 0.2 V. As revealed in Fig. 3e, the ORR activities for Fe-PyNG exhibited a slower attenuation with high current retention (91.3 %) after 5000 cycles than the Fe-PG catalyst (80.5 %). In contrast, a commercial Pt/C electrode showed a much faster current decrease with ~60 % retention. The better durability of Fe-PyNG can be ascribed to the strong coupling interaction of pyridine-N and Fe ion, which can suppress the dissolution, and facilitate the electron transfer. The Fe-PyNG electrocatalyst was further subjected to testing for methanol crossover toward ORR through its chronoamperometric responses

compared with Fe-PG and commercial Pt/C. Fig. 3f shows that the ORR current for Fe-PyNG remains unchanged after the subsequent addition of methanol, whereas that for Fe-PG, a slight change occurred. In contrast, a remarkable decrease for Pt/C is detected after the addition of methanol under the same testing conditions. The

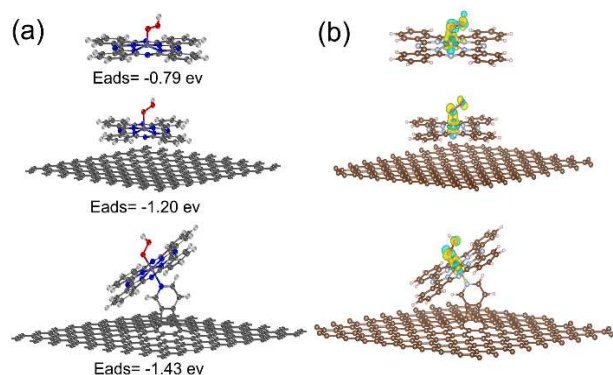


Fig. 4 (a) Optimized structure and adsorption energy of OOH on FePc, Fe-PG, and Fe-PyNG; (b) Induced charge rearrangements upon adsorption of OOH on FePc, Fe-PG, and Fe-PyNG. Blue (yellow) isosurfaces indicate depletion (addition) of $0.036 \text{ e}^-/\text{\AA}^3$.

results from both activity and stability studies indicate that Fe-PyNG is a desirable hybrid material toward ORR.

The adsorption of OOH on FePc, Fe-PG, and Fe-PyNG was investigated using spin-polarized DFT calculations, as shown in Fig. 4. The adsorption energy of OOH on FePc is -0.79 eV, which is in agreement with previously reported values^{29, 38}. When FePc is supported on graphene either in weak van der Waals (vdW) interaction or strong chemical bonding, a stronger OOH adsorption on Fe-PG (-1.20 eV) and Fe-PyNG (-1.43 eV) than that on FePc was observed. The bond distances of oxygen–oxygen of OOH adsorbed on FePc, Fe-PG, and Fe-PyNG are 1.12, 1.51 and 1.51 Å, respectively, implying that OOH is easily activated when adsorbed on FePc that is supported on graphene. OOH adsorption on five coordinate Fe of Fe-PyNG is much stronger (-1.43) than the four coordinate Fe of FePc (-0.79) and Fe-PG (-1.20). Based on Bader charge analysis results, the charge of Fe on Fe-PyNG is more positive than those on FePc and Fe-PG, which is also seen in Fig. 4b and S15. This finding indicates that the electron transfer from Fe to N in PyNG leads to a more positive charge of Fe on Fe-PyNG than those on FePc and Fe-PG. Therefore, N-modified Fe becomes a superior catalytic active site for a series of reactions as the ortho-carbon in various N-doped carbon materials.

The outstanding stability of Fe-PyNG during ORR in alkaline media is mainly caused by the following aspects: the strong chemical bonding between FePc and pyridine in PyNG, which ensures that the adsorbed molecules (e.g., OOH) cannot induce a large geometric change in FePc (Fig. 4), and the strong chemical bonding between pyridine and graphene, which makes FePc-pyridine a stable species on graphene. The weak π - π interaction between FePc and graphene leads to a worse stability than that of the Fe-PyNG system.

Conclusions

In summary, this study shows a design concept for fabricating Fe-PyNG hybrid via strong coupling between FePc and pyridine-N.

The prominent features of the Fe-PyNG hybrid include high electrocatalytic activity, superior durability, and better performance than Pt/C toward ORR in alkaline media. These features potentially make Fe-PyNG an outstanding nonprecious metal cathode catalyst for fuel cells. The incorporation of Fe ion and pyridine-N afforded effective bonding and synergetic coupling effects, which lead to significant electrocatalytic performance. DFT calculations indicate that N-modified Fe is a superior site for OOH adsorption and ORR reaction. Meanwhile, the strong chemical bonding between FePc and pyridine in PyNG, as well as between pyridine and graphene leads to its superior stability. We believe that our present synthetic strategy can be further extended to develop other metal complexes/N-doped carbon materials for broad applications in the field of catalysts, batteries, and supercapacitors.

Acknowledgements

This work was supported by National Basic Research Program of China (973 Program) (2013CB733501), the National Natural Science Foundation of China (NSFC-21306169, 21176221, 21136001, 21101137 and 91334103), Zhejiang Provincial Natural Science Foundation of China (ZJNSF-R4110345) and the New Century Excellent Talents in University Program (NCET-10-0979). We thank Prof. Youqun. Zhu for Instruments support.

Notes and references

^a College of Chemical Engineering, Zhejiang University of Technology, Hangzhou 310014 (China), E-mail: jgw@zjut.edu.cn

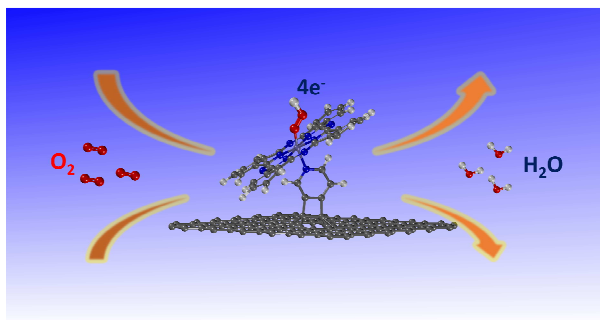
^b Institute for Integrated Catalysis, Pacific Northwest National Laboratory, Richland, Washington 99352, United States

† Electronic Supplementary Information (ESI) available: Detailed experimental procedures, additional characterizations, electrochemical measurements and computational calculation results. See DOI: 10.1039/c000000x/

1. M. K. Debe, *Nature*, 2012, **486**, 43-51.
2. J. Tollefson, *Nature*, 2010, **464**, 1262-1264.
3. N. Demirdoven and J. Deutch, *Science*, 2004, **305**, 974-976.
4. J. Wu and H. Yang, *Acc. Chem. Res.*, 2013, **46**, 1848-1857.
5. S. Guo, S. Zhang and S. Sun, *Angew. Chem. Int. Ed.*, 2013, **52**, 8526-8544.
6. G. Wu and P. Zelenay, *Acc. Chem. Res.*, 2013, **46**, 1878-1889.
7. H. Wang, T. Maiyalagan and X. Wang, *ACS Catal.*, 2012, **2**, 781-794.
8. D. S. Su and G. Sun, *Angew. Chem. Int. Ed.*, 2011, **50**, 11570-11572.
9. Z. Chen, D. Higgins, A. Yu, L. Zhang and J. Zhang, *Energy Environ. Sci.*, 2011, **4**, 3167-3192.
10. F. Jaouen, E. Proietti, M. Lefevre, R. Chenitz, J.-P. Dodelet, G. Wu, H. T. Chung, C. M. Johnston and P. Zelenay, *Energy Environ. Sci.*, 2011, **4**, 114-130.
11. Y. Zheng, Y. Jiao, M. Jaroniec, Y. Jin and S. Z. Qiao, *Small*, 2012, **8**, 3550-3566.
12. S. J. Yoo, S. J. Hwang, J.-G. Lee, S.-C. Lee, T.-H. Lim, Y.-E. Sung, A. Wieckowski and S.-K. Kim, *Energy Environ. Sci.*, 2012, **5**, 7521-7525.
13. R. Jasinski, *Nature*, 1964, **201**, 1212-1213.
14. S. Gupta, D. Tryk, I. Bae, W. Aldred and E. Yeager, *J. Appl. Electrochem.*, 1989, **19**, 19-27.
15. E. Proietti, F. Jaouen, M. Lefevre, N. Larouche, J. Tian, J. Herranz and J. P. Dodelet, *Nat. Commun.*, 2011, **2**, 416.
16. R. Bashyam and P. Zelenay, *Nature*, 2006, **443**, 63-66.

17. M. Lefèvre, E. Proietti, F. Jaouen and J.-P. Dodelet, *Science*, 2009, **324**, 71-74.
18. G. Wu, K. L. More, C. M. Johnston and P. Zelenay, *Science*, 2011, **332**, 443-447.
19. X. Chen, S. Sun, X. Wang, F. Li and D. Xia, *J. Phys. Chem. C*, 2012, **116**, 22737-22742.
20. W. Orellana, *J. Phys. Chem. C*, 2013, **117**, 9812-9818.
21. S. Sun, N. Jiang and D. Xia, *J. Phys. Chem. C*, 2011, **115**, 9511-9517.
22. F. Calle-Vallejo, J. I. Martinez and J. Rossmeisl, *Phys. Chem. Chem. Phys.*, 2011, **13**, 15639-15643.
23. Y. Liang, Y. Li, H. Wang and H. Dai, *J. Am. Chem. Soc.*, 2013, **135**, 2013-2036.
24. Y. Liang, Y. Li, H. Wang, J. Zhou, J. Wang, T. Regier and H. Dai, *Nat. Mater.*, 2011, **10**, 780-786.
25. D.-W. Wang and D. Su, *Energy Environ. Sci.*, 2014, **7**, 576-591.
26. Y. Jiang, Y. Lu, X. Lv, D. Han, Q. Zhang, L. Niu and W. Chen, *ACS Catal.*, 2013, **3**, 1263-1271.
27. C. Zhang, R. Hao, H. Yin, F. Liu and Y. Hou, *Nanoscale*, 2012, **4**, 7326-7329.
28. G. Dong, M. Huang and L. Guan, *Phys. Chem. Chem. Phys.*, 2012, **14**, 2557-2559.
29. R. Cao, R. Thapa, H. Kim, X. Xu, M. Gyu Kim, Q. Li, N. Park, M. Liu and J. Cho, *Nat. Commun.*, 2013, **4**, 2076.
30. M. Jahan, Q. Bao and K. P. Loh, *J. Am. Chem. Soc.*, 2012, **134**, 6707-6713.
31. X. Zhong, H. Yu, G. Zhuang, Q. Li, X. Wang, Y. Zhu, L. Liu, X. Li, M. Dong and J.-g. Wang, *J. Mater. Chem. A*, 2014, **2**, 897-901.
32. A. B. Sorokin, *Chem. Rev.*, 2013, **113**, 8152-8191.
33. K. Watanabe, H. Kitagishi and K. Kano, *Angew. Chem., Int. Ed.*, 2013, **52**, 6894-6897.
34. H. Peng, Z. Mo, S. Liao, H. Liang, L. Yang, F. Luo, H. Song, Y. Zhong and B. Zhang, *Sci Rep*, 2013, **3**, 1765.
35. K. Artyushkova, B. Kiefer, B. Halevi, A. Knop-Gericke, R. Schlögl and P. Atanassov, *Chem. Commun.*, 2013, **49**, 2539-2541.
36. R. Kothandaraman, V. Nallathambi, K. Artyushkova and S. C. Barton, *Appl Catal B-Environ*, 2009, **92**, 209-216.
37. G. Wu, C. M. Johnston, N. H. Mack, K. Artyushkova, M. Ferrandon, M. Nelson, J. S. Lezama-Pacheco, S. D. Conradson, K. L. More, D. J. Myers and P. Zelenay, *J. Mater. Chem.*, 2011, **21**, 11392-11405.
38. R. Chen, H. Li, D. Chu and G. Wang, *J. Phys. Chem. C*, 2009, **113**, 20689-20697.

Graphic abstract



Iron phthalocyanine (FePc) coordinated with pyridyne cycloaddition of graphene sheets (PyNG) as a high-performance electrocatalyst for ORR were fabricated.